Available online at www.sciencedirect.com
SCIENCE DIRECT®
International Journal of Thermal Sciences 43 (2004) 1037–1046
International Journal of Thermal Sciences
www.elsevier.com/locate/ijts

An optimised instrument to measure thermal diffusivities of gases with opto-acoustic spectroscopy

J. Soldner, K. Stephan *

Institute of Technical Thermodynamics and Thermal Process Engineering, University of Stuttgart, Pfaffenwaldring 9, 70550 Stuttgart, Germany

Received 10 December 2003; received in revised form 8 March 2004; accepted 8 March 2004

Available online 25 May 2004

Abstract

The paper describes the theory and application of opto-acoustics to determine thermal diffusivities of gases. An experimental device, already described in previous papers of the authors [Internat. J. Thermophys. 19 (1998) 1099; Proc. 2nd European Thermal Science and 14th UIT National Heat Transfer Conf., 1996, pp. 1071–1078] permitted the detection of thermal diffusivities of gases at moderate pressures with an experimental uncertainty of about ±1.25%.Based on the experience gained with this device, a comprehensive error analysis is presented in this paper. It shows how the experimental uncertainties can be considerably reduced to about −0.45 to +0.35%. The parameters for optical cell design are dealt with, as well as the appropriate characteristics, such as frequencies of the modulated laser beam, and the microphone used in the experiment.

Keywords: Opto-acoustics; Photo-acoustics; Thermal diffusivities; Thermal conductivity; Photo-acoustic cell

1. Introduction

The generation of acoustic signals from light energy, known as the opto- or photoacoustic effect, has become a promising method to study optical and thermophysical properties of condensed matter see, e.g., [1,2]. Its discovery goes back to the year 1881, when Alexander Graham Bell [3] first described the effect to transfer sound over distances of about 40 m. Further development was hampered, mainly because acoustic signals were too weak. It was then around 1937/38 when the effect experienced a renaissance with the invention of the ultrared absorption recorder [4,5], an instrument to measure concentrations of gases like CO, NO, SO_2 and others. The opto-acoustic spectroscopy then became an efficient tool for the detection of surface defects in materials [6–12], the detection of oil contamination in water supplies [13] and trace gas detection [4,5,14–20].

In recent years it was also used to determine thermophysical properties, such as thermal diffusivities and thermal conductivities of gases. With the aid of an opto-acoustic cell, developed in the laboratory of the authors [21–23] thermal diffusivities of refrigerants R134a and R32 were measured in the temperature range between ambient temperature and 363 K at low pressures with an experimental uncertainty of about ±1.25%.

Though this uncertainty comes close to that of the best instruments available at present to measure thermal diffusivities, the experience gained with the actual opto-acoustical cell permits the conclusion that the experimental error can still be reduced with optimised cell geometry and with appropriate characteristics of the incoming light. Such an optimisation requires a careful and comprehensive error analysis of the opto-acoustic instrument. It is the purpose of this paper to present such an analysis and from that deduce an optimised design and those experimental parameters that will lead to a higher accuracy.

2. Experimental set-up

The experimental set-up was already described elsewhere [22,23]. We therefore can confine ourselves on a short description of the principles. In the experiments a periodically modulated laser beam penetrates the sample chamber, Fig. 1, charged with the fluid to be tested. Small amounts of the radiative energy are absorbed by the test gas, provided that this gas absorbs infrared light of the emission wave length of the

* Corresponding author.
E-mail address: stephan@itt.uni-stuttgart.de (K. Stephan).

1290-0729/$ – see front matter
doi:10.1016/j.ijthermalsci.2004.03.003

Nomenclature

A	heat production	$W{\cdot}m^{-3}$
a	thermal diffusivity, $=\lambda/\rho c_V$	$m^2{\cdot}s^{-1}$
B	coefficient, Eq. (14)	
C^*	parameter, Eq. (4)	
C_m	constant, Eqs. (5)–(8)	
c_V	isochoric specific heat capacity	$J{\cdot}kg^{-1}{\cdot}K^{-1}$
d	diameter	m
d_{Ch}	chopper frequency	m
d_b	beam diameter	m
f	frequency	s^{-1}
I	intensity of laser beam	$W{\cdot}m^{-2}$
J_0, J_1	Bessel function of order zero and one	
K	number of periods	
k_f	coefficient, Eqs. (11) and (12)	
k_m	amplification factor	$V{\cdot}Pa^{-1}$
L	length	m
n	exponent	
p	pressure	Pa
$\dot{Q}$	heat flow	W
$\dot{q}$	heat flux	$W{\cdot}m^{-2}$
R	radius of sample chamber	m
	individual gas constant	$J{\cdot}kg^{-1}{\cdot}K^{-1}$
r	radial coordinate	m
T	temperature	K
$\overline{T}$	volume averaged temperature	K
t	time	s
V	volume	m^{-3}
v	specific volume	$m^3{\cdot}kg^{-1}$
v_{Ch}	circumferential speed of chopper blade	$m{\cdot}s^{-1}$
W	laser power	W
w	Gaussian beam radius	m
w_0	Gaussian beam radius at $z=0$	m
z_R	Rayleigh length	m

Greek symbols

α	absorption coefficient	m^{-1}
Δp	pressure difference	Pa
Δr	distance beam-cell axis	m
ΔT	temperature difference	K
$\Delta\hat{\vartheta}$	maximal temperature difference	K
$\Delta\bar{\vartheta}$	volume averaged temperature difference	K
Δt	jitter, Fig. 8	s
ζ_m	eigenvalues of Bessel function $J_0(\zeta_m)=0$	
φ	circumferential angle	
λ	thermal conductivity	$W{\cdot}m^{-1}{\cdot}K^{-1}$
Λ	wave length	m
ρ	density	$kg{\cdot}m^{-3}$
ϑ	temperature difference $T-T_0$	K
τ	time constant	s

Subscripts

0	initial or boundary value (at t, r or $z=0$)
∞	infinity ($t\to\infty$)
e	end value
H	back ground signal
id	ideal
W	wall

Superscripts

$+$	dimensionless quantity
D	dark phase
H	light phase

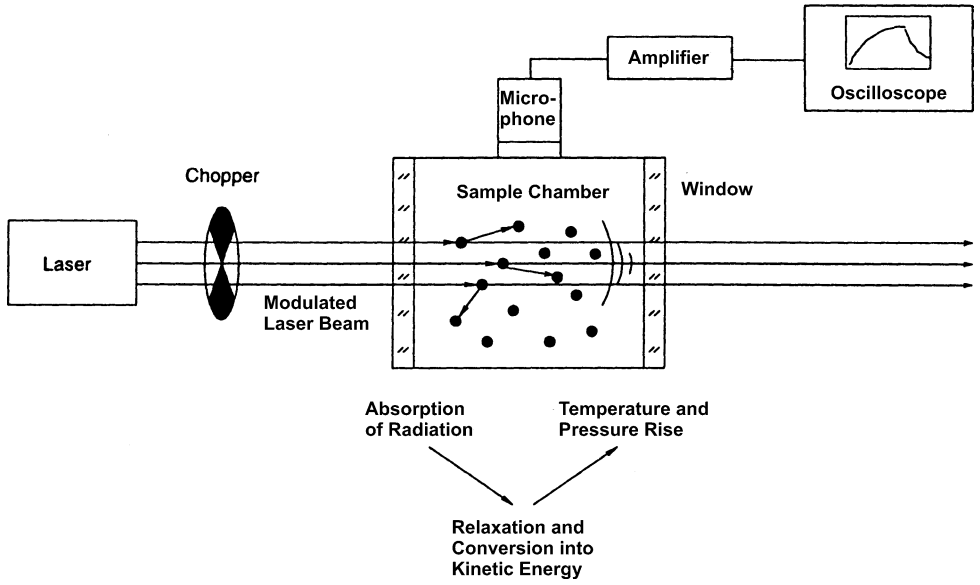

Fig. 1. Experimental set-up principle.

laser. Should this not be the case, some ppm of an absorbent may be added to the test gas, so that the thermophysical properties of the test gas remain unaffected within the experimental uncertainty. The energy absorption of gas provokes a small temperature rise of a few mK and a pressure rise in the isochoric cell of a few Pa. Because the laser beam is modulated periodically with a chopper, light phases are followed by dark phases, thus causing pressure fluctuations inside the gas. These fluctuations are recorded by a microphone. As they are related to the temperature fluctuations which depend on the thermal diffusivity, the instrument delivers directly, without preceding calibration, absolute values of the thermal diffusivities and thus is a "primary instrument" as defined by Kestin and Wakeham [24].

In a non-resonant cell, as discussed in the following, the microphone is mounted close to the cell wall. If it were placed farther away from the cell wall, a resonant cell would be created in form of a Helmholtz resonator. The pressure signal would be superseded by damped harmonic oscillations of the gas between sample chamber and microphone membrane, and experimental results would become less accurate.

3. The working equation

For reasons of completeness the working equation will shortly be derived here. A more detailed derivation was given by the authors elsewhere [21]. The equation assumes the gas in the sample chamber to be homogeneous and of constant density. It is true that density differences due to the temperature oscillations are inevitable. They propagate, however, with speed of sound and are equalised in the small chamber in some microseconds, whereas measurements are performed in a much longer time of some milliseconds. Furthermore, because of the high length to diameter ratio of the cell of about 68 in our case, axial temperature gradients can be neglected. The axis of the sample chamber coincides with that of the laser beam, which itself is rotational-symmetric. Under these assumptions the working equation reads

$$\frac{\partial \vartheta}{\partial t} = a\frac{1}{r}\frac{\partial}{\partial r}\left(r\frac{\partial \vartheta}{\partial r}\right) + \frac{A(r,z)}{\rho c_v} \tag{1}$$

$\vartheta(t,r,z) := T(t,r,z) - T_0$ denotes the difference between the gas temperature $T(t,r,z)$ and wall temperature T_0, ρ the gas density, c_v the isochoric heat capacity, r the radial and z the axial co-ordinate, $a := \lambda/\rho c_v$ is the thermal diffusivity defined with c_v because of the constant volume of the cell. The heat source

$$A(r,z) = \alpha I(r,z) \tag{2}$$

is given by the absorption coefficient α of the gas, and the intensity of the laser beam

$$I(r,z) = \frac{W}{\pi w^2(z)}\exp\left(-\frac{r^2}{w^2(z)}\right) \tag{3}$$

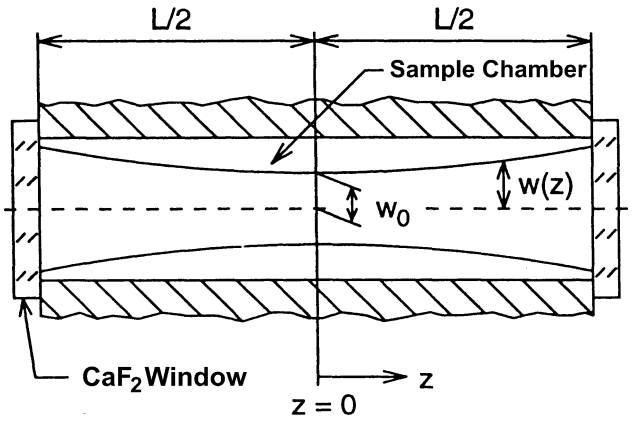

Fig. 2. Contour of an ideal Gaussian laser beam.

with the radiative power W (SI-unit W) and the Gaussian beam radius

$$w(z) = w_0\left(1 + C^* z^2\right)^{1/2} \tag{4}$$

The z co-ordinate has its origin in the focus, and w_0 is the beam radius in the focus, Fig. 2. The beam radius w_0 is defined as the radius where the beam intensity is $1/e$ of the peak intensity. The constants w_0 and C^* are determined experimentally with the aid of a beam profiler.

The boundary conditions for solving Eq. (1) are:
Constant wall temperature:

$$\vartheta(t, r = R, z) = 0$$

Zero initial temperature:

$$\vartheta(t = 0, r, z) = 0$$

and rotational symmetry:

$$(\partial\vartheta/\partial r)_{t,r=0,z} = 0$$

Introducing dimensionless quantities $r^+ = r/R$, $z^+ = z/R$, $w^+ = w/R$ and $t^+ = at/R^2$, the solution of Eq. (1) fulfilling the boundary conditions reads [21]

$$\vartheta\left(t^+, r^+, z^+\right) = \frac{\alpha W}{4\pi\lambda}\left\{\sum_{n=1}^{\infty}\frac{(-1)^n}{nn!(w^+)^{2n}}\left[\left(r^+\right)^{2n} - 1\right] + \sum_{m=1}^{\infty} C_m J_0\left(\zeta_m r^+\right)\exp\left(-\zeta_m^2 t^+\right)\right\} \tag{5}$$

with

$$C_m = -\frac{2}{J_1^2(\zeta_m)}\left\{\sum_{n=1}^{\infty}\frac{(-1)^n}{nn!(w^+)^{2n}} \times \int_{r^+=0}^{1}\left(\left(r^+\right)^{2n+1} - r^+\right)J_0\left(\zeta_m r^+\right)\mathrm{d}r^+\right\} \tag{6}$$

J_0 and J_1 are the Bessel functions of the zeroth and first order, and the eigenvalues ζ_m are to be determined from $J_0(\zeta_m) = 0$.

As illustrated in Fig. 3 each light phase is followed by a dark phase. During the dark phase the heat generation term

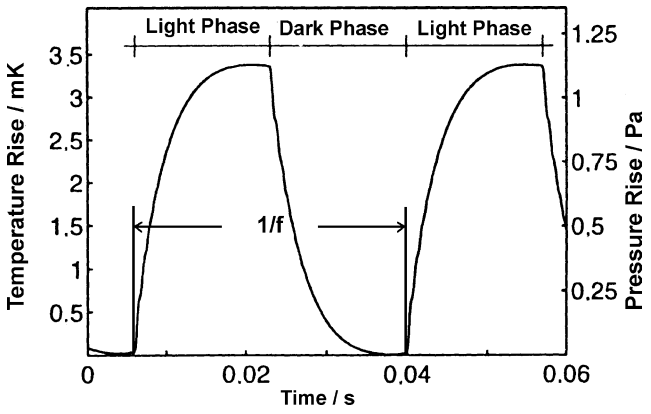

Fig. 3. Temperature and pressure in the test gas as function of time.

in Eq. (1) disappears. The boundary conditions remain unchanged, so that the temperature-rise under the assumption that the dark phase starts at $t^+ = 0$ becomes

$$\vartheta\left(t^+, r^+, z^+\right) = \frac{\alpha W}{4\pi\lambda} \sum_{m=1}^{\infty} C_m^D J_0\left(\zeta_m r^+\right) \exp\left(-\zeta_m^2 t^+\right) \tag{7}$$

The temperature-rise at the beginning of the dark phase at $t^+ = 0$ from Eq. (7) is identical with that at the end of the light phase from Eq. (5) with $t^+ = t_1^+ = a/(2fR^2)$ where f is the frequency of consecutive pairs consisting of a light and a dark phase. Thus equating Eq. (7) at $t^+ = 0$ with Eq. (5) at $t^+ = t_1^+$, multiplying then both sides with $r^+ J_0(\zeta_m r^+)$ and integrating between $r^+ = 0$ and $r^+ = 1$ delivers the constant C_m^D of Eq. (7):

$$C_m^D = -C_m\left[1 - \exp\left(-\zeta_m^2 t_1^+\right)\right] \tag{8}$$

The temperature at the beginning of the next light phase follows again from the solution of Eq. (1). When shifted over the time $t_1^+ = a/(2fR^2)$ it starts again at $t^+ = 0$, when the temperature is identical with that at the end of the previous dark phase. Repeating this procedure for the following phases we eventually obtain the temperature rise of light phase K, $K > 1$, preceded by $K - 1$ periods of light phases:

$$\begin{aligned}\vartheta = \frac{\alpha W}{4\pi\lambda}\Bigg\{ &\sum_{n=1}^{\infty} \frac{(-1)^n}{nn!(w^+)^{2n}}\left[\left(r^+\right)^{2n} - 1\right] \\ &+ \sum_{m=1}^{\infty} C_m\Bigg[1 - \sum_{k=1}^{K-1}\left\{\exp\left(-\zeta_m^2 t_1^+(2k-1)\right)\right. \\ &\left. - \exp\left(-2\zeta_m^2 t_1^+ k\right)\right\}\Bigg] \\ &\times J_0\left(\xi_m r^+\right)\exp\left(-\zeta_m^2 t^+\right)\Bigg\}\end{aligned} \tag{9}$$

The average temperature-rise

$$\bar{\vartheta}\left(t^+\right) := \int_V \vartheta\left(t^+, r^+, z^+\right) \mathrm{d}V \tag{10}$$

is related to pressure-rise registered by the microphone through the equation of state $p = p(\bar{\vartheta}, v)$. From a Taylor series expansion, with $v = \text{const}$ in our case, neglecting terms of higher order because of the small pressure rise of a few *Pa*, we obtain

$$\Delta p(t) = p(t) - p_0 = \left(\frac{\partial p}{\partial \bar{\vartheta}}\right)_v \bar{\vartheta}\left(t^+\right)$$

and

$$\Delta p(t \to \infty) = \Delta p_\infty = \left(\frac{\partial p}{\partial \bar{\vartheta}}\right)_v \bar{\vartheta}_\infty$$

and hence

$$\frac{\Delta p(t)}{\Delta p_\infty} = \frac{\bar{\vartheta}(t^+)}{\bar{\vartheta}_\infty}$$

After Integration of Eq. (10) with the aid of Eq. (9) we obtain from this the working equation, derived also in [21]:

$$\frac{\Delta p(t^+)}{\Delta p_\infty} = 1 + \sum_{m=1}^{\infty} K_m \exp\left(-\zeta_m^2 t^+\right) \cdot k_f\left(t_1^+\right) \tag{11}$$

with

$$\begin{aligned}k_f\left(t_1^+\right) = 1 - \sum_{k=1}^{K-1}\Big\{&\exp\left(-\zeta_m^2 t_1^+(2k-1)\right) \\ &- \exp\left(-2\zeta_m^2 t_1^+ k\right)\Big\}\end{aligned} \tag{11.1}$$

and

$$K_m = D_m/B \tag{12}$$

with

$$D_m = 4\int_{z^+=0}^{1/2}\int_{r^+=0}^{1} C_m\left(z^+\right) J_0\left(\zeta_m r^+\right) \mathrm{d}r^+ \,\mathrm{d}z^+ \tag{13}$$

and

$$B = 2\int_{z^+=0}^{1/2} \sum_{n=1}^{\infty} \frac{(-1)^{n+1}}{(n+1)!(w^+)^{2n}} \,\mathrm{d}z^+ \tag{14}$$

$C_m(z^+)$ follows from Eq. (6), and $w^+ = w^+(z^+)$ follows from Eq. (4). Because the pressure $\Delta p(t)$ is registered by the microphone the only unknown in the working Eq. (11) is the thermal diffusivity a included in $t^+ = at/R^2$ and in $t_1^+ = a/(2fR^2)$. Convergence of Eq. (11) with deviations below 0.001% is attained for $m \geqslant 6$, and a cyclic steady state is reached for a number of periods $K \geqslant 3$–20 depending on the thermal diffusivity.

4. Error analysis

The working equation (11) does not allow for some additional effects influencing the microphone signal and hence the thermal diffusivity determined from the experiments. Such effects come from: Clearance volume in front of the

microphone, deformation of the microphone membrane, absorption of light at the wall of the sample chamber, non-constant wall temperature, errors in the parameters describing the laser beam, and deviation of the beam axis from the cell axis. Minimising these errors will permit us to optimise the experimental set-up. The errors are discussed in the following.

4.1. Clearance volume

In a non-resonant cell, as studied here, the microphone is mounted at the wall of the sample chamber. Nevertheless, a clearance volume in front of the microphone membrane cannot be avoided entirely. Furthermore, microphones are equipped with a capillary tube connecting both sides of the membrane in order to equalise the static pressure exerted on both sides of the membrane. The clearance volume and the mass flow through the capillary tube induce changes of the gas density in the sample chamber during pressure-rise so that the assumption of a constant density in the working Eq. (7) is violated. These effects were studied in a previous paper [21]. It turned out that the effects can be considerably reduced, if the capillary tube is kept closed by a valve during the experiments, and if this valve is opened only when the sample chamber is filled or emptied with gas. As an error analysis revealed, the membrane should be mounted as close to the wall, so that the clearance volume is lower than 1% of the volume of the sample chamber. The resulting error in the thermal diffusivity is then as low as -0.2%.

4.2. Deformation of the microphone membrane

The assumption of a constant density in the working Eq. (7) presupposes that volume changes do not occur during the experiments. Actually, during the experiments the microphone membrane is exposed to pressure differences and the membrane deformations are recorded to measure the pressure differences. The real pressure change then obeys the thermal equation of state $p = p(\bar{\vartheta}, V)$ with $V \neq \text{const}$ instead of $V = \text{const}$ as assumed in the working Eq. (7). Thus the pressure change is given by

$$\Delta p(t) = \left(\frac{\partial p}{\partial \bar{\vartheta}}\right)_V \bar{\vartheta}(t) + \left(\frac{\partial p}{\partial V}\right)_{\bar{\vartheta}} \Delta V(t) \tag{15}$$

On the other hand the microphone will be chosen so, that deformation is in the range of elasticity. Then deformations and hence volume changes are linear functions of the pressure difference

$$\Delta V = \text{const}\,\Delta p$$

As an example we had $\text{const} = 8.687 \times 10^{-14}\ \text{m}^5\cdot\text{N}^{-1}$ for the microphone used in our experiments according to the manufacturer (Brüel and Kjaer, (1/2)″—microphone 4193). With this, Eq. (15) converts into

$$\Delta p(t)\left[1 - \left(\frac{\partial p}{\partial V}\right)_{\bar{\vartheta}} \text{const}\right] = \left(\frac{\partial p}{\partial \bar{\vartheta}}\right)_V \bar{\vartheta}$$

Thus the basis

$$\frac{\Delta p(t^+)}{\Delta p_\infty} = \frac{\bar{\vartheta}(t^+)}{\bar{\vartheta}_\infty}$$

of the working Eq. (7) is still valid. The deformation of the microphone membrane does not affect the thermal diffusivities determined from the experiments.

4.3. Wall absorption of light

Even in cases when the sample chamber is filled with a non-absorbing gas, for instance a noble gas or nitrogen, we obtain an opto-acoustical signal, because part of incoming light is absorbed at the wall of the sample chamber. This provokes a wall temperature-rise and thus a heat flux from the wall to the gas. As a consequence an additional pressure-rise is registered as a *background signal* overlapping the main signal. To minimise this signal the wall of the sample chamber should be polished. As recommended by Zharov and Letokhov [10] the background signal can be determined with the aid of a reference cell, mounted in parallel or in series with the test cell and filled with a non-absorbing gas. The laser beam passes both cells, and the background signal from the reference cell is subtracted from the signal of the test cell.

Instead of this we preferred to determine the background signal in pre-tests with a non-absorbing gas and describe this signal analytically with the aid of the following model.

The variation of wall temperature $\Delta\vartheta_w$ with time t should satisfy the following conditions:

(i) For $t \to 0$ the slope $\mathrm{d}\Delta\vartheta_w/\mathrm{d}t$ is finite, and
(ii) For $t \to \infty$ we have $\mathrm{d}\Delta\vartheta_w/\mathrm{d}t = 0$. The wall temperature approaches a maximum value $\Delta\hat{\vartheta}_w$.

Thus it is plausible to assume

$$\frac{\mathrm{d}\Delta\vartheta_w}{\mathrm{d}t} = k_w \frac{\Delta\hat{\vartheta}_w}{\tau} \exp(-t/\tau) \tag{16}$$

where τ is a time-constant depending on the design of the sample chamber. The factor k_w depends on the frequency f, and we have $k_w(f = 0) = 1$. k_w decreases with increasing frequency, because wall temperature oscillations become smaller the higher the frequency. Thus we have $k_w(f) \leqslant 1$. Integration of Eq. (16) with the initial condition $\Delta\vartheta_w(t = 0) = 0$ delivers

$$\Delta\vartheta_w = k_w \Delta\hat{\vartheta}_w\left[1 - \exp(-t/\tau)\right] \tag{17}$$

In analogy to Eq. (11), where k_F according to Eq. (11.1) describes the influence of $K - 1$ light phases on the gas pressure of phase K, we may formulate

$$k_w = 1 - \sum_{k=1}^{K-1} \left\{ \exp\left(-\frac{2k-1}{2f\tau}\right) - \exp\left(-\frac{k}{f\tau}\right) \right\} \tag{18}$$

The maximum temperature $\Delta\hat{\vartheta}_w$ and the time-constant τ depend on design and amount of light absorbed by the wall, and must to be adapted to the experiments.

The background temperature-rise $\Delta\vartheta_H$ of the gas obeys the energy equation

$$\frac{\partial\Delta\vartheta_H}{\partial t} = a\frac{1}{r}\frac{\partial}{\partial r}\left(r\frac{\partial\Delta\vartheta_H}{\partial r}\right) \tag{19}$$

The boundary conditions are $\Delta\vartheta_H(t=0)=0$, $\Delta\vartheta_H(r=R)=\Delta\vartheta_W$ from Eq. (17), and $\frac{\partial\Delta\vartheta_H(r=0)}{\partial r}=0$.

Introducing dimensionless co-ordinates $t^+ = at/R^2$, $\tau^+ = a\tau/R^2$ and $r^+ = r/R$ we obtain the background temperature-rise[1]

$$\begin{aligned}\Delta\vartheta_H\left(t^+,r^+\right) &= k_W\Delta\hat{\vartheta}_W\left\{1-2\sum_{m=1}^{\infty}\left(\frac{1}{\zeta_m}-\frac{\zeta_m}{\zeta_m^2-1/\tau^+}\right)\right.\\ &\quad\times\frac{J_0(\zeta_m r^+)}{J_1(\zeta_m)}\exp\left(-\zeta_m^2 t^+\right)\\ &\quad\left.-\frac{J_0(\sqrt{r^{+2}/\tau^+})}{J_0(\sqrt{1/\tau^+})}\right\}\end{aligned} \tag{20}$$

The average background temperature-rise of the gas

$$\Delta\bar{\vartheta}_H\left(t^+\right) = 2\int_{r^+=0}^{1}\Delta\vartheta_H\left(t^+,r^+\right)r^+\,\mathrm{d}r^+$$

follows from this as

$$\begin{aligned}\Delta\bar{\vartheta}_H(t^+) &= k_W\Delta\hat{\vartheta}_W\left\{1-4\sum_{m=1}^{\infty}\left(\frac{1}{\zeta_m^2}-\frac{\zeta_m}{\zeta_m^2-1/\tau^+}\right)\right.\\ &\quad\times\exp\left(-\zeta_m^2 t^+\right)\\ &\quad\left.-\frac{2J_1(\sqrt{1/\tau^+})}{(\sqrt{1/\tau^+})J_0(\sqrt{1/\tau^+})}\exp\left(-\frac{t^+}{\tau^+}\right)\right\}\end{aligned} \tag{21}$$

again with ζ_m from $J_0(\zeta_m)=0$.

From $\Delta\bar{\vartheta}_H(t^+)$ we obtain the background pressure-rise

$$\Delta p_H(t) = \left(\frac{\partial p}{\partial\bar{\vartheta}_H}\right)_\rho\Delta\bar{\vartheta}_H(t) \tag{22}$$

with $(\partial p/\partial\bar{\vartheta}_H)_\rho = R\rho$ for an ideal gas. This pressure-rise $\Delta p_H(t)$ adds to the pressure rise of the working equation, Eq. (11). The time constant τ and the maximum temperature-rise $\Delta\bar{\vartheta}_w$ in Eq. (20) are properties of the test cell filled with a non-absorbing gas. Hence, these values when determined once, can be used for different test gases. With our experimental set-up we found with Argon as test gas a maximum temperature rise of $\Delta\hat{\vartheta}=0.449$ mK and a time constant $\tau = 8.47$ ms.

Fig. 4 shows as an example a background signal recorded in Volt with Argon as test gas for two initial pressures $p_0 = 0.096$ MPa and $p_0 = 0.0522$ MPa and a temperature $T_0 = 304$ K. The amplification factor is 0.709 Pa·V^{-1}. The

[1] The solution of Eq. (19) under the given boundary conditions can also be found in the book of Tautz [25] when superimposing his Eq. (5.28) with his Eq. (11.97).

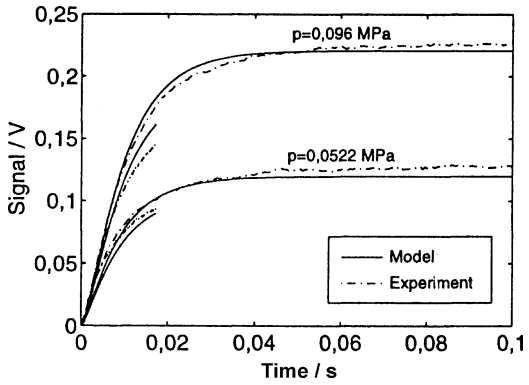

Fig. 4. Background signal. Argon as test gas, 0.096 MPa and 0.0522 MPa at $T_0 = 304$ K, $f = 5$ and 29 s^{-1}.

experiments agree very well with those obtained from our model Eqs. (21) and (22). Though the experiments were made with frequencies $f = 5$ s^{-1} and $f = 29$ s^{-1} the results were almost independent of frequency. This follows also from Eq. (18), wherefrom we obtain almost the same values of factor k_w, $k_w(f = 5\text{ s}^{-1}) = 0.992$ and $k_w(f = 29\text{ s}^{-1}) = 0.998$. Nevertheless it is recommended to determine the parameters $\Delta\hat{\vartheta}_w$ and τ in pre-tests with the same chopper frequencies as in the subsequent experiments.

4.4. Fluctuation of the wall temperature

In order to find out how fluctuations of the wall temperature, caused, for example, by the thermostat, may affect the thermal diffusivity determined in the experiments, we postulate a sudden linear increase of the wall temperature $\vartheta_w = T_w - T_0$ from its initial value $\vartheta_w(t=0)=0$ over a time of $t_e = 20$ ms. The end temperature $\vartheta_{\mathbf{we}} = (\mathrm{d}\vartheta/\mathrm{d}t)_{t=0}t_e$ depends on the slope $(\mathrm{d}\vartheta/\mathrm{d}t)_{t=0}$, which was varied between $\pm 7.5\times10^{-5}$ K·s^{-1} and $\pm 2.5\times10^{-3}$ K·s^{-1}. With that the pressure-rise Δp becomes different from the pressure signal Δp_{id} calculated from the working equation, Eq. (11), assuming constant wall temperature. As an example Fig. 5 presents values $(\Delta p - \Delta p_{\mathrm{id}})/\Delta p_{\mathrm{id}}$ for a slope $(\mathrm{d}\vartheta/\mathrm{d}t)_{t=0} = 7\times10^{-4}$ K·s^{-1}. The thermal diffusivity attributed to the pressure signal Δp is about $\pm 0.25\%$ different from the thermal diffusivity attributed to Δp_{id}, meaning that a temperature fluctuation of $\pm 7\times10^{-4}$ K·s^{-1} causes an error of $\pm 0.25\%$ in the thermal diffusivity.

With our experimental device wall temperatures were recorded every 15 s, and fluctuations during that time interval were below ± 1 mK. Thus the maximum slope was ± 1 mK/15 s $= \pm 6.7\times10^{-5}$ K·s^{-1} leading to an experimental uncertainty in the thermal diffusivity below $\pm 0.05\%$.

4.5. Laser beam parameters

The parameter C^* in Eq. (4) depends on the Rayleigh-length $z_R = \pi w_0^2/\Lambda$ according to $C^* = 1/z_R^2$ and can be determined very precisely. Λ is the wave length of the laser

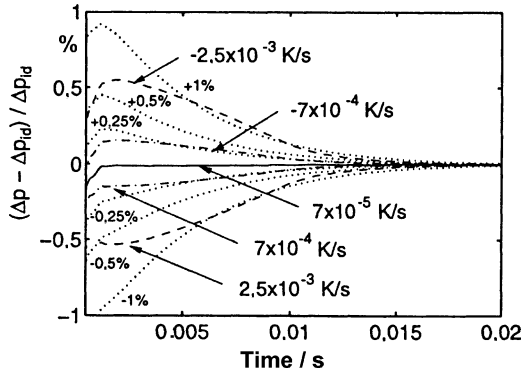

Fig. 5. Sensitivity analysis. Linear increase of wall temperature. Argon as test gas 0.1015 MPa, $T_0 = 304$ K.

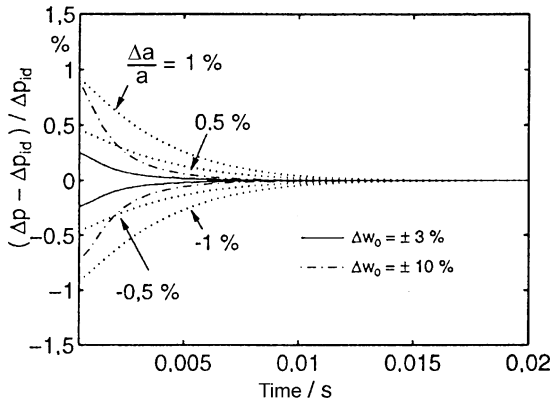

Fig. 6. Sensitivity analysis. Change of gaussian beam radius Δw_0. Argon as test gas 0.1015 MPa, $T_0 = 304$ K.

beam. In our case we found $C^* = 0.1571 \times 10^{-3}$ m^{-2}. The beam radius w_0, however, determined with a Laser-diagnostic system has uncertainties of ±3%. As shown in Fig. 6 this causes an error in the pressure signal Δp when determined from the working equation, Eq. (11), with a beam radius $w_0 \pm 0.03 w_0$, compared to the pressure signal Δp_{id} that would be obtained if the beam radius were w_0, solid line in Fig 6. Almost the same curves would be obtained if the thermal diffusivities had an uncertainty of ±0.25%.

4.6. Deviation of beam axis from cell axis

The working equation, Eq. (11), presupposes coinciding axes of laser beam and sample chamber. Non-parallel axes deliver too high thermal diffusivities. If axes are parallel and a distance Δr apart from each other, errors in the thermal diffusivity are higher than in the case of oblique axes. When axes are parallel, the intensity, Eq. (3), depends on the distance Δr of the axes and their circumferential angle φ. We have then $I(r, \Delta r, \varphi, z)$. For this case Biermann [26] solved the energy equation. The deviation in pressure as calculated by him is plotted in Fig. 7. It clearly indicates that significant errors can arise when the axes of the laser beam and the sample chamber do not coincide. The error

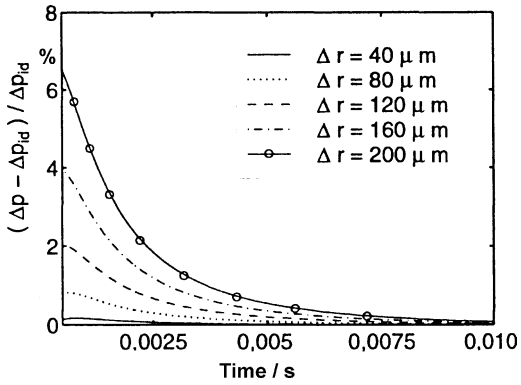

Fig. 7. Sensitivity analysis. Different distances Δr between beam axis and cylinder axis of sample chamber. Argon as test gas, 0.1015 MPa, $T_0 = 304$ K.

maximum is at the beginning of each light phase and tends to zero for $t \to \infty$. In our experiments both axes were about 40 μm apart from each other. The uncertainty in the thermal diffusivity then is +0.25% at the beginning of the light phase. It disappears almost after 0.01 s, which requires frequencies below $f = 25$ s^{-1}. The light phase lasts then more than 0.01 s. Provided that the pressure then is registered during a time interval between 5×10^{-3} s to 0.01 s, the uncertainty in the thermal diffusivity is below 0.1%. Because of the higher error made when pressure signals are recorded in the beginning of the light phase, it is recommended to omit those signals and use preferentially the signals recorded towards the end of the light phase.

4.7. Mechanical chopper blade

When passing from a dark to a light phase, the laser beam because of its finite diameter does not immediately penetrate the gas in the sample chamber with full intensity. It takes a small but finite time until the laser beam is set free by the rotating chopper plate. The time to set the laser beam entirely free is

$$\Delta t_0 = \frac{d_b}{v_{\mathrm{Ch}}} = \frac{d_b}{(d_{\mathrm{Ch}}/2)\pi f}$$

where d_b is the beam diameter and $v_{\mathrm{Ch}} = (d_{\mathrm{Ch}}/2)\pi f$ the circumferential speed of the chopper blade of diameter d_{Ch}. The chopper blade generates two periods during one turn. With $d_b = 0.74$ mm and $d_{\mathrm{Ch}} = 110$ mm in our experiment we obtain

$$\Delta t_0 = 4.28 \times 10^{-3}/f \tag{23}$$

It takes about 0.43% of the period duration until the laser beam is set entirely free. The *centre of intensity* of the laser beam when set free by the chopper blade is shifted over a distance corresponding to half the beam diameter, which is equivalent to the case of a laser beam not coaxial with the axis of the sample chamber. This corresponds to a shift

$$\Delta r = \frac{w_0}{2}\frac{\Delta t_0}{\Delta t_1} = \frac{2 d_b w_0}{d_{\mathrm{ch}}\pi}$$

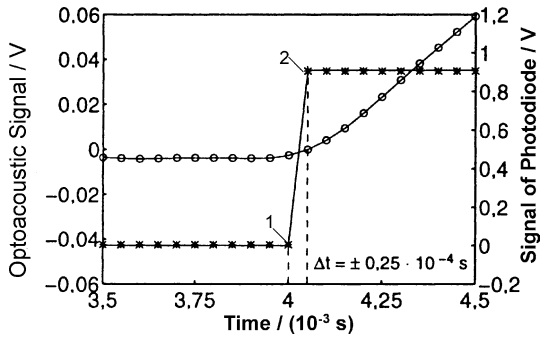

Fig. 8. Optoacoustic signal ○ and signal of photodiode * from experiments.

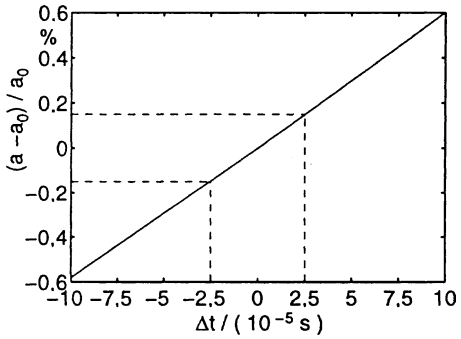

Fig. 9. Error in thermal diffusivity due to Jitter Δt of Fig. 8.

where Δt_0 is the time to set the laser beam free, and Δt_1 is the time of a light phase. With Δt_0 from Eq. (23), $\Delta t_1 = 1/2f$, $d_b = 0.74$ mm, $d_{\mathrm{ch}} = 110$ mm and $w_0 = 0.166$ mm we obtain $\Delta r = 0.71$ μm leading to an additional, however negligible error in the thermal diffusivity of 0.005%.

The opto-acoustic signal at the beginning and at the end of a light phase is registered by a photodiode placed in the ray path at the outlet of the sample chamber. Both signals, that of light phase and the opto-acoustical signal are recorded simultaneously. As shown in Fig. 8, the chopper starts to set the laser beam free at point 1, and at point 2 it is entirely free. The upper curve represents the opto-acoustical signal, recorded simultaneously. The jitter Δt, defined as time interval between point 2 and point 1, is 0.25×10^{-4} s. Instead of time $t^+ = at/R^2$ the working equation (11) contains now a time $\tilde{t}^+ = a(t - \Delta t)/R^2$. With the experimental data $\Delta p(t)/\Delta p_\infty$ we can then fulfil the working equation when adapting the thermal diffusivity via a parameter optimisation. As a result, Fig. 9, shows the error $(a - a_0)/a_0$ of thermal diffusivity a for a given jitter Δt from the value a_o that would be obtained when the jitter disappeared. For a jitter of $\Delta t = 0.25 \times 10^{-4}$ s the error in the thermal diffusivity is about 0.15%.

This error can be avoided almost entirely with an optical chopper, which, different from the mechanical chopper permits an intermediate transition from the dark to the light phase.

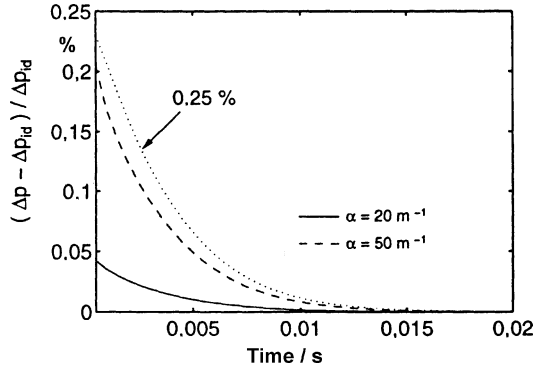

Fig. 10. Sensitivity analysis. Pressure signal when absorption coefficient is high, $\alpha = 20$ m^{-1} and 50 m^{-1}. Thermal diffusivity $a = 3.59 \times 10^{-5}$ m^2·s^{-1}.

4.8. Axial heat conduction

As long as absorption coefficients of the test gas are low, for example below 0.5 m^{-1}, axial heat conduction is negligible. Many test gases are, however, strong absorber for certain wave lengths of the incoming light. Then the absorption rate along the axial co-ordinate may not be assumed constant. The Lambert–Beer law instead of Eq. (3) now reads

$$I(r,z) = \frac{W}{\pi w^2(z)} \exp\left(-\frac{r^2}{w^2(z)}\right) \exp(-\alpha z) \tag{24}$$

The laser power absorbed per volume is

$$A(r,z) = \alpha I(r,z)$$

and the energy equation reads

$$\frac{\partial \vartheta}{\partial t^+} = \frac{1}{r^+}\frac{\partial}{\partial r^+}\left(r^+ \frac{\partial \vartheta}{\partial r^+}\right) + \frac{1}{L^{+2}}\frac{\partial^2 \vartheta}{\partial z^{+2}} + \frac{A(r,z)R^2}{\lambda} \tag{25}$$

with the dimensionless quantities $t^+ = at/R^2$, $L^+ = L/R$, $z^+ = z/L$ and the temperature $\vartheta = T - T_0$.

The boundary conditions are $\vartheta(t^+ = 0) = \vartheta(r^+ = 1) = \vartheta(z^+ = -1/2) = \vartheta(z^+ = +1/2) = 0$ and $(\partial\vartheta/\partial r^+)_{r^+=0} = 0$.

The length ratio $L^+ = L/R$, of cell length L over cell radius R is very large, in our case $L^+ = 104\,\mathrm{mm}/0.765\,\mathrm{mm} = 1.355 \times 10^2$ and hence $1/L^{+2} = 5.446 \times 10^{-5}$. This indicates that axial temperature gradients according to Eq. (25) are of weak influence on the temperature field. From a numerical solution of Eq. (25) with the boundary conditions given above, we obtain the temperature field $\vartheta(t^+, r^+, z^+)$ and from this the volume averaged temperature $\bar{\vartheta}(t^+)$, which itself is related to the pressure rise $\Delta p(t)$ because of $\Delta p(t)/\Delta p_\infty = \bar{\vartheta}(t)/\bar{\vartheta}_\infty$. As a result of the numerical analysis, Fig. 10 shows the relative deviation of pressure $\Delta p(t)$ when axial heat conduction is taken into account, and $\Delta p_{\mathrm{id}}(t)$ when it is neglected, as a function of time for absorption coefficients $\alpha = 20$ m^{-1} and 50 m^{-1}. From an error analysis we find for $\alpha = 20$ m^{-1} an error of about 0.25% in the thermal diffusivity, dotted line in Fig. 10.

Substances like the fluorinated methane- and ethane derivatives, utilised as ozone-safe refrigerants, are strong absorbers at wavelengths of about 3400 nm [27]. Depending on pressure, absorption coefficients of about 50 m^{-1} were registered. In this case axial heat conduction cannot be neglected. On the other hand most often absorption coefficients are mostly unknown. However, wavelengths were substances are small absorbers or do not absorb at all are easy to determine. Then a good absorber tracer gas with well known absorption coefficients may be added to the substance to be tested. Transmission spectra of some refrigerants, such as R134a, R32 and R152a, show that these substances at pressures above 0.2 MPa do not absorb at a wavelength of 1531 nm. At this wavelength ammonia is a strong absorber and might serve as a tracer gas. Tuneable laser diodes, particularly in the near infrared of wavelengths between 100 nm and 1700 nm are commercially available. They can be tuned to the wavelengths of ammonia or other tracer gases.

4.9. Optimal chopper frequency

As shown before the pressure rise $\Delta p(t)$ approaches its limiting value Δp_∞ after an infinite time $t \to \infty$ of a light phase. This is experimentally not feasible. Instead it is reasonable to choose a chopper frequency so that a light phase ends at a time when $\Delta p = (0.8 \text{ to } 0.9) \cdot \Delta p_\infty$ is reached. When it ends earlier, the curvature of the signal $\Delta p(t)$ recorded with the microphone is large, and thus the error in the thermal diffusivities when determined with the aid of the working equation, Eq. (11), is high. Inserting

$$\frac{\Delta p(t = 1/2f)}{\Delta p_\infty} \geqslant 0.85$$

into the working equation, Eq. (11), the equation converts into a relation with chopper frequency and thermal diffusivity as unknown variables. When using only the first eigenterm we obtain as an approximation with $k_p(t_1^+) = 1$ for the first light phase

$$\frac{\Delta p(t = 1/2f)}{\Delta p_\infty} = 0.85 = 1 + K_1 \exp\left(-\frac{\zeta_1^2 a}{2fR^2}\right) \tag{26}$$

With the values $K_1 = -1.0793$ from Eqs. (12)–(14) and $\zeta_1 = 2.4048$ from $J_0(\zeta_1) = 0$, we obtain

$$\frac{fR^2}{a} = 1.465 \tag{27}$$

as an approximate formula to estimate the optimal frequency for given values of the cell radius R. If, for example, we estimate the thermal diffusivity of the test gas to $a = 10^{-6}$ $m^2 \cdot s^{-1}$, we obtain for a cell diameter $2R = 1.535$ mm an optimal frequency of $f \cong 2.5$ s^{-1}, and for a cell diameter $2R = 3$ mm, $f \cong 0.65$ s^{-1}. With our microphone pressure fluctuations between $0.12 \text{ s}^{-1} < f < 1000 \text{ s}^{-1}$ could be recorded. Thus the cell with 1.535 mm in diameter allowed thermal diffusivities to be measured in the range of

$$5 \times 10^{-8} \text{ m}^2 \cdot \text{s}^{-1} \leqslant a \leqslant 4 \times 10^{-4} \text{ m}^2 \cdot \text{s}^{-1}$$

Table 1
Experimental uncertainties with present cell and uncertainties expected with optimised cell. Test gas Argon, 304 K, 0.1015 MPa

Error source	Uncertainties in %, present cell, diameter 1.535 mm	Uncertainties in %, optimised cell, diameter 3 mm
Clearance volumes	−0.6	−0.2
Wall absorption, wall temperature fluctuations	±0.05	0
Laser beam parameters	±0.25	±0.05
Deviation from cell axis	0 to +0.1	0 to 0.1
Mechanical chopper blade	±0.15	–
Optical chopper	–	0
Registration of pressure	±0.2	±0.2
Total uncertainty	−1.25 to +0.75	−0.45 to +0.35

whereas with a cell of 3 mm in diameter the range would be

$$2 \times 10^{-7} \text{ m}^2 \cdot \text{s}^{-1} \leqslant a \leqslant 1.5 \times 10^{-3} \text{m}^2 \cdot \text{s}^{-1}$$

Thermal diffusivities of technically relevant gases are in this range.

4.10. Experimental uncertainty

The following table summarises the experimental uncertainties of the thermal diffusivities. As shown before axial heat conduction can be avoided when measurements are made in a weak or non-absorbing region, if a tracer gas is added. Deformation of the microphone membrane turned out to be unimportant. Wall absorption, leading to a background signal, can be compensated. As Table 1 shows for Argon as an example, the total uncertainty reached with our sample chamber of 1.525 mm diameter and 104 mm length lies between −1.25 and +0.75%.

The uncertainties can be reduced with a sample chamber of the same length, but wider diameter. However, some disadvantages when using a cell with wider diameter cannot be ignored: The pressure-rise of the test gas then becomes slower, necessitating a lower chopper frequency. There exists a maximal chopper frequency given by the lowest frequency of microphone and amplifier. As shown before a reduction of chopper frequencies leads to a shift of the region in which thermal diffusivities can be measured. On the other hand, when using a wider diameter, the error due to wall absorption almost disappears, because the radial intensity of the laser beam decays exponentially with distance from the wall. A good compromise seems to be a diameter of 3 mm: The wall absorption becomes negligible, and as shown in the previous chapter the range of experiments in which thermal diffusivities can be measured is still wide enough.

For further reduction of the experimental uncertainties an optical chopper is recommended in the optimised cell.

5. Conclusions

The opto-acoustic technique is an efficient tool to determine thermal diffusivities of gases. Because of the low temperature gradients produced in the test gases, experimental errors due to radiation and convection are extremely small and negligible. The method was used to determine thermal diffusivities and from them thermal conductivities of gases in the low density range, where other well proved methods, such as the transient hot wire method or the photon- correlation spectroscopy, become less accurate. It should however be possible to extend the application of the opto-acoustic method to higher densities, because available microphones permit experiments with fluids of higher density.

As a result of the error analysis presented in this paper, measures to improve the experimental accuracy were proposed. It turned out that a main source of the experimental uncertainties comes from

- The clearance volume between sample chamber and microphone membrane,
- The fluctuation of wall temperatures,
- The determination of laser beam parameters with a laser diagnostic system,
- The deviation of beam axis from cell axis,
- The mechanical chopper blade, and
- The registration of pressure.

As the analysis of these error-sources revealed the most important errors can be considerably reduced. The clearance volume becomes lower when the microphone membrane is placed into the wall of the sample chamber. New laser-diagnostic systems deliver very accurate laser beam parameters, and an optical instead of the mechanical chopper blade avoids the chopper blade error.

Wall absorption and wall temperature fluctuations become negligible with a cell of 3 mm in diameter instead of 1.535 mm, because wall absorption of the laser beam decays exponentially with distance from the wall. With such an optical cell thermal diffusivities, a, can be determined in a wide range of $2 \times 10^{-7}\ \mathrm{m^2{\cdot}s^{-1}} \leqslant a \leqslant 1.5 \times 10^{-3}\ \mathrm{m^2{\cdot}s^{-1}}$.

From an approximate formula, Eq. (27), the optimal chopper frequency for a given value of the cell diameter and the expected thermal diffusivity can be estimated.

References

[1] A. Rosencwaig, A. Gersho, Theory of the photoacoustic effect of solids, J. Appl. Phys. 47 (1976) 64–69.
[2] A. Rosencwaig, Photoacoustics and Photoacoustic Spectroscopy, Wiley, New York, 1980.
[3] A.G. Bell, On the production and reproduction of sound by light, Amer. J. Sci. 20 (1880) 305–324.
[4] K.F. Luft, Über eine neue Methode der registrierenden Gasanalyse mit Hilfe der Absorption ultraroter Strahlen ohne spektrale Zerlegung, Z. Tech. Phys. 24 (1943) 97–104.
[5] E. Lehrer, K.F. Luft, Verfahren zur Bestimmung von Bestandteilen in Stoffgemischen mittels Strahlenabsorption. German Patent DE 730478.
[6] J.F. Mc Clelland, R.W. Jones, S.J. Bajic, FT-IR photoacoustic spectroscopy, in: J.M. Chalmers, R.R. Griffiths (Eds.), Handbook of Vibrational Spectroscopy, Wiley, New York, 2002.
[7] D. Kumar, S.P. McGlynn, Role of photoacoustic in optogalvanics, J. Chem. Phys. 93 (6) (1990) 3899–3906.
[8] J. Pelzl, K. Klein, O. Nordhaus, Extended Helmholtz resonator in low-temperature photoacoustic spectroscopy, Appl. Optics 21 (1992) 94–99.
[9] W. Demtröder, Laser-Spectroscopy-Basic Concepts and Instrumentation, Springer, Berlin, 1986.
[10] V.P. Zharov, V. Letokhov, Laser Optoacoustic Spectroscopy, Springer, Berlin, 1986.
[11] P. Korpion, B. Büchner, On the thermodynamics of the photoacoustic effect of condensed matter in gas cells, Appl. Phys. B 30 (1983) 121–129.
[12] M.J.D. Low, G.A. Parodi, Infrared photoacoustic spectroscopy of solids and surface species, Appl. Spectr. 34 (1980) 76–80.
[13] J. Mortylewski, B. Wišlicki, K. Krawczyk, E. Kotlicka, Photoacoustic investigation of contaminated working fluids, Anal. Sci. 17 (2001) 425–427.
[14] L.B. Kreuzer, C.K.N. Patel, Nitric oxide air pollution: detection by optoacoustic spectroscopy, Science 173 (1971) 45–47.
[15] K. Stephan, W. Hurdelbrink, Die photoakustische Infrarot-Laser Spektroskopie zur Konzentrationsmessung in Gasen, Chem.-Ing.-Techn. 58 (1986) 485–487.
[16] M. Fehér, Y. Jiang, J.P. Maier, A. Miklós, Optoacoustic trace—gas monitoring with near-infrared diode laser, Appl. Optics 33 (9) (1994) 1655–1658.
[17] J.G. Parker, D.N. Ritke, Collisional deactivation of vibrationally excited singlet molecular oxygen, J. Chem. Phys. 59 (1973) 3173–3722.
[18] R. Klein, P. Hess, Untersuchung der Schwingungsrelaxation von Methan und Tetrafluormethan beim Stoß mit Wasserstoff, Deuterium und Edelgasen, Acustica 33 (1975) 198–202.
[19] M. Huetz-Aubert, F. Lepoutre, G. Louis, Etude opto-acoustique de la relaxation vibrationelle de CH_4 (ν_4, ν_4) dans les Chocs CH_4–CH_4 et CH_4-monoatomiques, J. Phys. 38 (1977) 238–290.
[20] A. Karbach, P.J. Hess, Photoacoustic signal in a cylindrical resonator: Theory and laser experiments for CH_4 and C_2H_6, J. Chem. Phys. 84 (1986) 2945–2952.
[21] J. Soldner, K. Stephan, Analysis of the photoacoustic detector signal for thermal diffusivities of gases, Internat. J. Thermophys. 19 (4) (1998) 1099–1109.
[22] J. Soldner, K. Stephan, The photoacoustic technique: A method to determine thermal diffusivities of gases at moderate pressures, in: Proc. 2nd European Thermal Science and 14th UIT National Heat Transf. Conf., 1996, pp. 1071–1078.
[23] J. Biermann, K. Stephan, The Photoacoustic Technique as a Convenient Instrument to Measure Thermal Diffusivities of Gases, Internat. J. Heat Mass Transfer 35 (1992) 605–612.
[24] J. Kestin, W.H. Wakeham, Cindas Data Series on Material Properties, in: Transport Properties of Fluids: Thermal Conductivity, Viscosity and Diffusion Coefficient, vol. I-1, Hemisphere, New York, 1988.
[25] H. Tautz, Wärmeleitung und Temperaturausgleich, Verlag Chemie, Weinheim, 1971.
[26] J. Biermann, Ein photoakustisches Messverfahren zur Bestimmung der Temperaturleitfähigkeit von Gasen, Diss. Univ., Stuttgart, 1992.
[27] J.M. Soldner, Bestimmung der Temperaturleitfähigkeit von Gasen mit dem photoakustischen Effekt, in: Fortschritt—Berichte VDI, vol. 778, VDI, Düsseldorf, 1999.